Increasing hourly population exposure to moderate cold under climate warming

International Journal of Disaster Risk Science
https://doi.org/10.1007/s13753-026-00702-4

www.ijdrs.com
www.springer.com/13753

ARTICLE

Increasing Hourly Population Exposure to Moderate Cold Under Climate Warming

Hongzhou Zhu[1,2] · Yanjiao Wang[3] · Jianping Duan[3] · Cunde Xiao[3] · Buwen Dong[4] · Zhao-Liang Li[5,6] · Dabo Guan[7] · Fei Ge[8] · Haoxin Zhang[9] · Deliang Chen[7]

Accepted: 15 December 2025

Abstract

Although the human health risk from cold stress may be greater than from heat stress, population cold exposure has received little attention compared to heat exposure in the context of climate warming. A particular puzzle is that while the number of cold days has markedly decreased under climate warming, the cold-related influenza positivity rate has substantially increased. Here we reveal global hourly population exposure for different cold categories based on observations and climate model simulations from 1979 to 2100, and explore the potential link between population cold exposure and influenza positivity rate. Our results show that the number of cold hours did not decrease uniformly across all categories under climate warming, but shifted from extreme cold to moderate cold. Global hourly population cold exposure increased substantially from 1979 to 2023 (2.05×10^{10} person-hours yr^{-1}), and this trend is expected to persist in the near term with continued population growth. The number of influenza positives and the influenza positivity rate were significantly correlated with hourly population cold exposure. These findings imply a current risk of population cold exposure and emphasize the need for increased attention to this risk.

Keywords Climate warming · Cold stress · Hourly population exposure · Influenza

1 Introduction

Anomalous heat and cold stresses have adverse impacts on human life and health (The Eurowinter Group 1997; Gasparrini et al. 2015; Mora et al. 2017; Pennisi et al. 2020), and such impacts have drawn growing attention from both the scientific community and the general public (Sheridan and Allen 2015; Arnold et al. 2022; Fyke and Weaver 2023; Romanello et al. 2023). While climate warming has amplified heat-related harms (Kovats and Hajat 2008; Patz et al. 2005; Oudin Åström et al. 2013; Ebi et al. 2021; Zhu and Duan 2025), epidemiological evidence indicates that

✉ Jianping Duan
duanjp@bnu.edu.cn

1 CAS Key Laboratory of Regional Climate-Environment for Temperate East Asia, Institute of Atmospheric Physics, Chinese Academy of Sciences, Beijing 100029, China

2 University of Chinese Academy of Sciences, Beijing 101408, China

3 State Key Laboratory of Earth Surface Processes and Disaster Risk Reduction, Faculty of Geographical Science, Beijing Normal University, Beijing 100875, China

4 National Centre for Atmospheric Science, Department of Meteorology, University of Reading, Reading RG6 6BB, United Kingdom

5 State Key Laboratory of Efficient Utilization of Arid and Semi-arid Arable Land in Northern China, Institute of Agricultural Resources and Regional Planning, Chinese Academy of Agricultural Sciences, Beijing 100081, China

6 Laboratory of Resources and Environment Information System, Institute of Geographic Sciences and Natural Resources Research, Chinese Academy of Sciences, Beijing 100101, China

7 Department of Earth System Sciences, Tsinghua University, Beijing 100084, China

8 School of Atmospheric Sciences, Plateau Atmosphere and Environment Key Laboratory of Sichuan Province, Chengdu University of Information Technology, Chengdu 610225, China

9 State Key Laboratory of Severe Weather Meteorological Science and Technology, and Institute of Tibetan Plateau Meteorology, Chinese Academy of Meteorological Sciences, Beijing 100081, China

Published online: 23 February 2026

cold-related health issues and excess deaths may be an order of magnitude greater than those associated with heat (Gasparrini et al. 2015; Martínez-Solanas et al. 2021). Typically, cold stress can lead to hypothermia (Collins et al. 1985; Woodhouse et al. 1993), influenza (Ballester et al. 2016), cardiovascular, cerebrovascular, and respiratory diseases (Donaldson et al. 1998; Raatikka et al. 2007). However, compared with heat stress, much less attention has been paid to the study of population exposure to cold stress (Carmona et al. 2016; Paschalidou et al. 2017), due to the decreased number of extreme cold days under climate warming (Christiansen et al. 2018; van Oldenborgh et al. 2019; Zhang et al. 2022).

Population exposure to cold stress (hereafter cold exposure) can be expressed as a product of the duration of low temperature and size of the suffering population, and has been used as a metric to measure the risk of the population exposed to cold (Gao et al. 2019; Broadbent et al. 2020; Du et al. 2022). Previous study has analyzed regional cold exposure based on the number of cold days, concluding that cold exposure has decreased significantly over recent decades under climate warming (Gao et al. 2018). However, an hourly-based cold exposure projection in metropolitan regions of the United States highlighted that extreme cold exposure by 2100 would be marginally greater than that in 2000 under the RCP 8.5 scenario (Broadbent et al. 2020). Given the substantial regional differences in population and the number of cold hours, hourly-based global cold exposure analyses throughout historical and future periods are required to reveal the changes in cold exposure under climate warming.

A number of meteorological factors, including surface air temperature (SAT), humidity, wind speed, and radiation affect how the human body feels and human health (Carter-Templeton et al. 2022; Li et al. 2023). Under the combined influence of these factors, the physical condition of humans varies with different categories of cold stress (Bröde et al. 2012). Moderate cold, rather than extreme cold, can induce most cold-related health burdens (Raatikka et al. 2007; Gasparrini et al. 2015). In view of the complicated interaction between multiple meteorological factors and biophysical reactions, the Universal Thermal Climate Index (UTCI) has been considered a suitable metric for cold exposure analysis (Fiala et al. 2012; Havenith et al. 2012).

Among the human health hazards linked to cold exposure (Raatikka et al. 2007; Ballester et al. 2016; Zhao et al. 2021), influenza is a particularly widespread respiratory infection that has been proven to be significantly associated with meteorological factors (Shaman and Kohn 2009; Roussel et al. 2016). Typically, influenza epidemics occur in winter, with populations exposed to low temperatures and low humidity experiencing an increased risk of influenza transmission (Peci et al. 2019; Ference et al. 2020; Carter-Templeton et al. 2022). Notably, although the number of cold days has significantly decreased under climate warming (Peterson et al. 2013; Shi et al. 2018; Zhang, Ren, et al. 2019), the cold-related influenza positivity rate has increased (Zhang, Wang, et al. 2019; Chen et al. 2023). The cause of this mismatch remains unknown.

Here, we aim to reveal the changes in cold stress under climate warming, and to quantify hourly population exposure across distinct cold categories throughout historical and future periods spanning 1979−2100 under the shared socioeconomic pathway (SSP)2-4.5 scenario (O'Neill et al. 2016), as well as assessing associated health risks. Hourly SAT and UTCI are used to analyze hourly SAT-only-based and multi-variables-based cold exposure, along with well-validated and high spatiotemporal resolution population data from the Inter-Sectoral Impact Model Intercomparison Project 2b (ISI−MIP-2b) for the period 1979–2100 (Frieler et al. 2017). The relationship between cold exposure and influenza recorded in World Health Organization (WHO) FluNet database is also analyzed to explore the impact of cold exposure on human health.

2 Data and Methods

This section first introduces the characteristics and applicability of the data used, followed by a detailed description of the research methods, including the calculation of metrics, the methodology of attribution, and the correction of model simulations.

2.1 Hourly Climatic Data

In this section, we introduce the meteorological dataset used in this study and its related attributes, including the data period, spatial resolution, and reliability.

2.1.1 Surface Air Temperature Data of the Fifth Generation Reanalysis (ERA5) Dataset

The ERA5 hourly surface air temperature (SAT) dataset, provided at a $0.25° \times 0.25°$ spatial resolution, is available from 1940 onwards (Hersbach et al. 2020). In this study, we used the hourly ERA5 SAT data spanning the period from 1979 to 2023.

2.1.2 Universal Thermal Climate Index (UTCI) Dataset and Its Calculation

The UTCI was used as the second metric to measure cold stress, and hourly UTCI data were obtained from ERA5-HEAT (Di Napoli et al. 2020). The UTCI is defined as the air temperature (°C) that would cause the equivalent dynamic

physiological response under a set of reference conditions (Bröde et al. 2012). Reference conditions were referred to the following metrics: mean radiant temperature (T_{mrt}) = air temperature (°C); wind speed (10 m above ground level) (v_a) = 0.5 m/s; relative humidity (R_h) = 50% (SAT ≤ 29 °C); and water vapor pressure (e_a) = 20 hPa (SAT > 29 °C). The calculation can be conducted by the thermofeel package in Python (Brimicombe et al. 2022). The dataset has a spatial resolution of 0.25° × 0.25° and is available from 1940 onward. To match the period of ERA5 SAT data, we used UTCI data from 1979 to 2023 in this study.

2.1.3 Meteorological Station Data

Observed hourly records of SAT, wind speed, and relative humidity from 2400 Chinese meteorological stations obtained from the China Meteorological Administration (CMA 2017) were used to evaluate the hourly ERA5 SAT and UTCI datasets. All the station observations are homogenous and have been quality controlled by the CMA. Most of the station records cover the period of 1979−2020.

2.1.4 Modern-Era Retrospective Analysis for Research and Applications, Version 2 (MERRA-2) Hourly Surface Air Temperature (SAT) Data

Besides the assessment of hourly ERA5 SAT data based on observational records from meteorological stations in China, we also assessed the ERA5 SAT and ERA5 SAT-based cold exposure using another hourly gridded SAT dataset obtained from MERRA-2 (Gelaro et al. 2017). The MERRA-2 hourly SAT dataset has a spatial resolution of 0.5° × 0.625°, is available from 1980 onwards, and its high quality has been verified in previous studies (Gelaro et al. 2017; Luo et al. 2020; Wen et al. 2022).

2.1.5 Climate Model Simulations

To project the future hourly population cold exposure, we used hourly SAT data from the GFDL-ESM4 and MIROC-ES2L models participating in the Coupled Model Intercomparison Project Phase 6 (CMIP6) (Eyring et al. 2016). Since there are fewer hourly models in CMIP6, only these two models provide hourly SAT data for the complete historical period and SSP2-4.5 scenario. The MIROC-ES2L model provides 30 realizations of hourly SAT at 2.8° × 2.8° resolution for 1850–2014 (historical) and 2015–2100 (SSP2-4.5) (Hajima et al. 2020), while the GFDL-ESM4 model offers hourly SAT at 1° × 1.25° for 1980–2014 (historical, first realization) and 2015–2100 (SSP2-4.5, second and third realizations) (Dunne et al. 2020).

2.2 Population Data

We used the annual global population dataset from ISI-MIP (1860–2100) with a spatial resolution of 0.0833° × 0.0833° (Frieler et al. 2017). The historical and future population datasets originate from different sources and differ in their time period. The historical data were from 1860 to 2005, whereas the future data cover the period from 2010 to 2100 (Frieler et al. 2017). Therefore, the population data from 2006 to 2009 were lacking. For the data gap, we linearly merged the data to match the SSP2 data in 2010 (Geiger et al. 2021). Data for the period 1979–2100 were used in our cold exposure analysis. To maintain the spatial pattern of the population as precisely as possible, population data were upscaled to 0.1° × 0.1° by first-order conservative remapping, which can keep the total population the same in the process. Correspondingly, reanalysis and all CMIP6 data used were also downscaled to the same resolution via bilinear interpolation to match the population data.

2.3 Influenza Data

To explore the relationship between influenza and cold exposure, we used influenza positivity rate data from sentinel sites in China and the United States during 2015–2019, obtained from the WHO FluNet database (World Health Organization 2022). These countries have the most complete records of influenza positives and negatives. All influenza types were included in the analysis. To avoid the influence of the COVID-19 pandemic, data after 2020 were excluded (Jones 2021).

2.4 Comparison and Assessment of Hourly Surface Air Temperature (SAT) and Universal Thermal Climate Index (UTCI) Data

We performed an assessment of hourly ERA5 SAT and UTCI using meteorological station data from China. We first matched the nearest grids of ERA5 SAT and UTCI to the locations of meteorological stations. Given that some observational values were missing, we only extracted ERA5 SAT and UTCI data at time coordinates when station observations were complete. We then used bilinear interpolation to calculate the SAT and UTCI at the locations of the target stations, while eliminating the errors induced by elevation differences (Cosgrove et al. 2003). The hourly ERA5 SAT grid data were corrected using the following equation:

$$T = T_{\text{interped}} + \gamma \Delta Z \tag{1}$$

where T is the corrected ERA5 hourly SAT (°C) and T_{interped} is the interpolated value (°C); γ is the lapse rate (assumed to be 6.5 °C/km), and ΔZ is the elevation difference. The

Pearson correlation coefficient (R), root-mean-square error (RMSE), and symmetric mean absolute percentage error (SMAPE) were employed to assess the total number of cold (≤ 0 °C) hours of the corrected ERA5 SAT against the station observations. The results show high consistency, with most grid cells demonstrating strong correlations and low errors (Fig. S1[1]). Furthermore, ERA5-derived cold hours closely agree with those from MERRA-2 in both spatial distribution and temporal trends, with correlation coefficients exceeding 0.9 across most land areas and > 0.99 at the global scale during 1979–2023 (Fig. S2a–S2c[1]).

When validating the UTCI, there is an absence of station observations for the radiation components (that is, diffuse solar radiation at the surface). To evaluate the performance of the UTCI as thoroughly as possible, we used station observations for the variables of SAT, humidity, and wind speed, and set the T_{mrt} to be equal to the SAT according to the reference conditions of UTCI radiation (see Sect. 2.1.2). The interpolation method of the other gridded meteorological variables (that is, humidity and wind speed) used for UTCI evaluation was the same as that used for ERA5 SAT described above, and the output was referred to as UTCI*. The UTCI* calculated from ERA5 showed good agreement with that calculated from station observations (Fig. S1[1]).

2.5 Calculation of Cold Hours

The ERA5 SAT- and UTCI-based cold hours were divided into five categories: total number of cold hours (UTCI/SAT $\leq$ 0 °C), moderate cold hours ($-$ 13 °C < UTCI/SAT $\leq$ 0 °C), strong cold hours ($-$ 27 °C < UTCI/SAT $\leq -$ 13 °C), very strong cold hours ($-$ 40 °C < UTCI/SAT $\leq -$ 27 °C), and extreme cold hours (UTCI/SAT $\leq -$ 40 °C). For each category, the annual number of cold hours was calculated per grid cell, and the global mean was derived by averaging over grids where cold-hour occurrences were observed. To reveal the changing proportion of cold hours within a single cold day in different categories, the following formula was used:

$$P = \frac{\text{Hours}}{\text{Days}} \tag{2}$$

where P is the annual averaged proportion of cold hours in cold days at a specific cold category. Hours and Days are annual globally average numbers of cold hours and cold days. To reveal the spatial characteristics of cold hours, the spatial coverage percentage of cold hours in each category was also calculated by dividing the number of grids in which cold hours of a specific category occurred by the total number of global land grids.

2.6 Hourly Population Cold Exposure Calculation

Hourly cold exposure in a specific category is the product of the population and number of cold hours in a given grid (Broadbent et al. 2020). Meanwhile, national and global hourly cold exposures were calculated as the sum of hourly cold exposures occurring in all grids within a country and globally, respectively. Hourly cold exposure in weekly and yearly scales was calculated by the sum of cold exposure within a single week and year, respectively. Weekly hours of cold exposure per person were calculated by dividing the cold exposure in a specific country by the population in that country.

2.7 Attribution Analysis for Changes in Population Cold Exposure

According to the attribution method of population exposure proposed by Jones et al. (2015) and Tuholske et al. (2021), we decomposed the change in population exposure into climate, population, and interaction effects (Zhu and Duan 2025). For the climate effect, climate was allowed to change while population was fixed at the reference year (that is, 1979). The population effect was derived by allowing population to change while fixing climate at the reference year. The interaction effect corresponds to the remainder after subtracting the population and climate effects from the total exposures:

$$\Delta E = P_1 \times \Delta C + C_1 \times \Delta P + \Delta C \times \Delta P \tag{3}$$

where ΔE denotes the total change in exposure; C_1 and P_1 represent the number of cold hours and population in the fixed year, respectively; while ΔC and ΔP represent their changes relative to 1979. Following the approach of Tuholske et al. (2021), we defined the climate effect as $P_1 \times \Delta C$, the population effect as $C_1 \times \Delta P$, and the interaction effect as $\Delta C \times \Delta P$.

To quantify the contribution of each component, we calculated their relative proportions using regression coefficients estimated through ordinary least squares (OLS). Correspondingly, these three effects can be expressed as follows:

$$\text{Eff}_* = \alpha_* + \beta_* Y_i + \varepsilon_* \tag{4}$$

where Eff_* is the effect of climate, population, and interaction. α_*, β_*, and ε_* are intercept, regression coefficient, and residuals. The symbol * represent *cli*, *pop*, and *inter*, and Eq. 4 was applied to calculate the climate effect, population effect, and interaction effect, respectively.

[1] https://zenodo.org/records/18482954

On the basis of the regression coefficients above, the relative share of these three effects was defined as follows (if all are > 0):

$$\text{Share} = \frac{\beta_{\text{eff}}}{\beta_{\text{cli}} + \beta_{\text{pop}} + \beta_{\text{inter}}}, \beta_{\text{cli}}, \beta_{\text{pop}}, \beta_{\text{inter}} > 0, \text{eff} = \text{cli, pop, inter} \tag{5}$$

If any coefficients are ≤ 0, the share was defined first by the following cases based on the trend of cold exposure being negative:

$$\text{Share} = \begin{cases} \frac{\beta_1}{\beta_1+\beta_2}, \beta_1, \beta_2 < 0 \\ \frac{\beta_2}{\beta_1+\beta_2}, \beta_1, \beta_2 < 0 \\ 0\%, \beta_3 > 0 \end{cases} \tag{6}$$

where β_1, β_2, and β_3 are regression coefficients derived from Eq. 4, and the subscripts respectively correspond to one of the three: 1 = population (pop), 2 = climate (cli), and 3 = interaction effect (inter). According to the conditions of the formula, they can be substituted in the corresponding equality calculation.

Second, when cold exposure shows an increasing trend:

$$\text{Share} = \begin{cases} \frac{\beta_{\text{inter}}}{\beta_{\text{inter}}+\beta_2} = 0\%, \beta_{\text{inter}}, \beta_2 < 0 \\ \frac{\beta_2}{\beta_{\text{inter}}+\beta_2} = 0\%, \beta_{\text{inter}}, \beta_2 < 0 \\ 100\%, \text{ for eff3}, \beta_3 > 0 \end{cases} \tag{7}$$

This is similar to Eq. 6. The β_{inter} is negative, because according to the distributive law of multiplication, it must be negative in this case.

2.8 Relationship Analysis of Hourly Population Cold Exposure with Influenza

Based on the weekly number of influenza positives and negatives in China and the United States derived from the sentinel surveillance sites of the FluNet dataset, the weekly influenza positivity rate (*PR*) was calculated as follows:

$$\text{PR} = \frac{\text{Num}_{\text{pos}}}{\text{Num}_{\text{pos}}+\text{Num}_{\text{neg}}} \tag{8}$$

where Num_{pos} and Num_{neg} are the weekly number of positives and negatives, respectively. Correspondingly, weekly hours of cold exposure per person (see Sect. 2.6) were calculated for China and the United States. The OLS method was employed to disclose the relationships of the number of influenza cases and influenza positivity rate with hourly population cold exposure.

2.9 Assessment and Correction of Simulated Cold Hours

To examine the consistency of cold hours simulated by different realizations of the same climate model, we calculated correlation coefficients for both the temporal series and spatial distributions of total cold (≤ 0 °C) hours derived from the first 10 realizations of the MIROC-ES2L model in the historical period (1979−2014) and SSP2-4.5 period (2015−2100), and for the two realizations of GFDL-ESM4 during 2015–2100. Notably, GFDL-ESM4 during the historical period (1980−2014) has only one realization, thus the consistency examination cannot be performed. All correlation coefficients were significant at the 0.001 level (Tables S3−S6[1]). Thus, we used the first realization of the MIROC-ES2L model in both the historical period and the future period under the SSP2-4.5 scenario for further analysis. For the GFDL-ESM4 model, we used the first realization in the historical period and second realization (only the second and third realizations were available) in the future period under SSP2-4.5. We corrected the simulated cold hours based on the cumulative probability density function (CDF) of ERA5, and calculated the quantiles of ERA5- and simulation-based SAT in the historical period as follows:

$$\varepsilon_{i,\text{obs}} = F_{\text{obs}}\left[T_{\text{obs}}\right] \tag{9}$$

and

$$\varepsilon_{i,\text{Hsim}} = F_{\text{Hsim}}\left[T_{\text{Hsim}}\right] \tag{10}$$

where $\varepsilon_{i,\text{obs}}$ and $\varepsilon_{i,\text{Hsim}}$ are the quantile values (that is, i°C) of the observed SAT T_{obs} and simulated SAT $T_{\text{Hsim},h}$, respectively; F_{obs} and F_{Hsim} are the CDFs of ERA5- and simulation-based SAT, respectively. To correct the trend of cold hours in the simulations, the annual trends of quantile values at the same SAT for ERA5 and historical simulations were calculated using OLS:

$$T_{\text{Hsim},i} = \alpha_{\text{Hsim}} + \beta_{\text{Hsim}} Y_i + \varepsilon_{\text{Hsim}} \tag{11}$$

and

$$T_{\text{obs},i} = \alpha_{\text{obs}} + \beta_{\text{obs}} Y_i + \varepsilon_{\text{obs}} \tag{12}$$

where β_{Hsim} and β_{obs} are the trends of quantile values at i°C of SAT from historical simulations and ERA5, respectively.

We then corrected the mean of CDF of simulations at the same SAT of ERA5, and the mean of quantile values at the same SAT was derived from the time series of quantile values after detrending:

$$M_{\mathrm{Hsim}}(i) = \frac{\sum_{n=1}^{m} q_{\mathrm{Hsim},de(i)}}{Num_{\mathrm{year}}} \tag{13}$$

and

$$M_{\mathrm{obs}}(i) = \frac{\sum_{n=1}^{m} q_{\mathrm{obs},de(i)}}{Num_{\mathrm{year}}} \tag{14}$$

where $M_{\mathrm{Hsim}}(i)$ and $M_{\mathrm{obs}}(i)$ are the means of quantile values at i°C from the historical simulations and ERA5 after detrending, respectively; $\mathrm{Num}_{\mathrm{year}}$ refers to the number of years in the historical period.

Next, we corrected the CDF trend as follows:

$$\varepsilon_{i,\mathrm{Hsim,cor}} = \varepsilon_{i,\mathrm{Hsim}} + \Delta Tr_i + \Delta M_i \tag{15}$$

where $\varepsilon_{i,\mathrm{Hsim,cor}}$ is the quantile value at i°C after correction, and $\Delta Tr_i = T_{\mathrm{obs},i} - T_{\mathrm{Hsim},i}$ and $\Delta M_i = M_{\mathrm{obs}}(i) - M_{\mathrm{Hsim},}(i)$.

According to the $\varepsilon_{i,\mathrm{sim},h,\mathrm{cor}}$ in the historical period, quantile mapping was conducted as follows:

$$X_{\mathrm{Hsim}}(i) = F^{-1}_{\mathrm{Hsim,cor}}\left[\varepsilon_i\right] \tag{16}$$

where $F^{-1}_{\mathrm{Hsim,cor}}$ is the CDF after correction in Eq. 15. After this processing, the trend of total number of cold hours was shown to be well-corrected, with little difference in trend between the simulation and ERA5 SAT (Fig. S3[1]).

For corrections in the period 2015−2100, we retained the relative change and climate sensitivity of the SSP2-4.5 scenario using the quantile delta mapping method (Cannon et al. 2015). First, the trend and mean of quantile values at the same SAT of the SSP2-4.5 scenario were calculated, similar to Eqs. 11 and 13, as follows:

$$T_{\mathrm{Psim}}(i) = \alpha_{\mathrm{Psim}} + \beta_{\mathrm{Psim}}(i)Y_i + \varepsilon_{\mathrm{Psim}} \tag{17}$$

and

$$M_{\mathrm{Psim}}(i) = \frac{\sum_{n=1}^{m} q_{\mathrm{Psim},de(i)}}{\mathrm{Num}_{\mathrm{year}}} \tag{18}$$

where $\mathrm{Num}_{\mathrm{year}}$ is the number of years. The deltas of the mean and trend between the simulations derived from the projection period and historical period were calculated as follows:

$$\Delta_{i,PTr}(i) = T_{\mathrm{Psim}}(i) - T_{\mathrm{Hsim}}(i) \tag{19}$$

and

$$\Delta_{i,PM}(i) = M_{\mathrm{Psim}}(i) - M_{\mathrm{Hsim}}(i) \tag{20}$$

where $\Delta_{i,PTr}(i)$ and $\Delta_{i,PM}(i)$ are delta changes of trend and mean of CDFs in SSP2-4.5 relative to that in the historical period.

The correction of the CDF in the future period under SSP2-4.5 was calculated as follows:

$$\varepsilon_{i,\mathrm{Psim,cor}} = \varepsilon_{i,\mathrm{Psim}} + \left[\Delta_{i,PTr}(i) + T_{\mathrm{obs}}(i)\right] + \left[\Delta_{i,PM}(i) + M_{\mathrm{obs}}(i)\right] \tag{21}$$

where $\varepsilon_{i,\mathrm{Psim,cor}}$ is the corrected quantile value at i°C, and all quantile values after correction comprise the corrected annual CDF in the SSP2-4.5 projection $F_{\mathrm{obs},p,\mathrm{cor}}$. The corrected SAT was mapped as follows:

$$X^{\mathrm{cor}}_{\mathrm{Psim}}(i) = F^{-1}_{\mathrm{obs,Pcor}}\left[\varepsilon_i\right] \tag{22}$$

Thus, the bias of the number of cold hours in simulations was well-corrected.

3 Results

This section first clarifies the characteristics of changes in cold hours and their comparison with cold days. Then, population exposure based on cold hours is calculated. Furthermore, it analyzes and quantifies the factors causing changes in cold exposure. Finally, it explores the relationship between cold exposure and influenza and predicts future exposure to cold hours.

3.1 Changes in Cold Hours Under Climate Warming

Both annual cold hours and the proportion of cold hours within a single cold day have changed due to climate warming in recent decades (Fig. 1). Although the UTCI- and SAT-based cold hours in the categories of total cold, very strong cold, and extreme cold have decreased significantly over 1979–2023, the annual cold hours for both moderate cold and UTCI-based strong cold categories exhibit non-significant change over this period (Fig. 1). Notably, cold hours in the categories of moderate and strong cold account for a greater proportion of total cold hours compared to very strong and extreme cold (49% and 38% for SAT- and UTCI-based moderate cold, 33% and 40% for SAT- and UTCI-based strong cold, 27% and 29% for SAT- and UTCI-based very strong cold, and 8% and 29% for SAT- and UTCI-based extreme cold) (Fig. 1a–e).

A second notable finding is the increased proportion of UTCI-based cold hours within a single cold day for moderate, strong, and very strong cold categories under the background of climate warming over recent decades (Fig. 1g–i). Meanwhile, the UTCI-based proportion of extreme and total cold hours within a single cold day showed a significant decrease (Fig. 1j and 1f), and changes in other categories

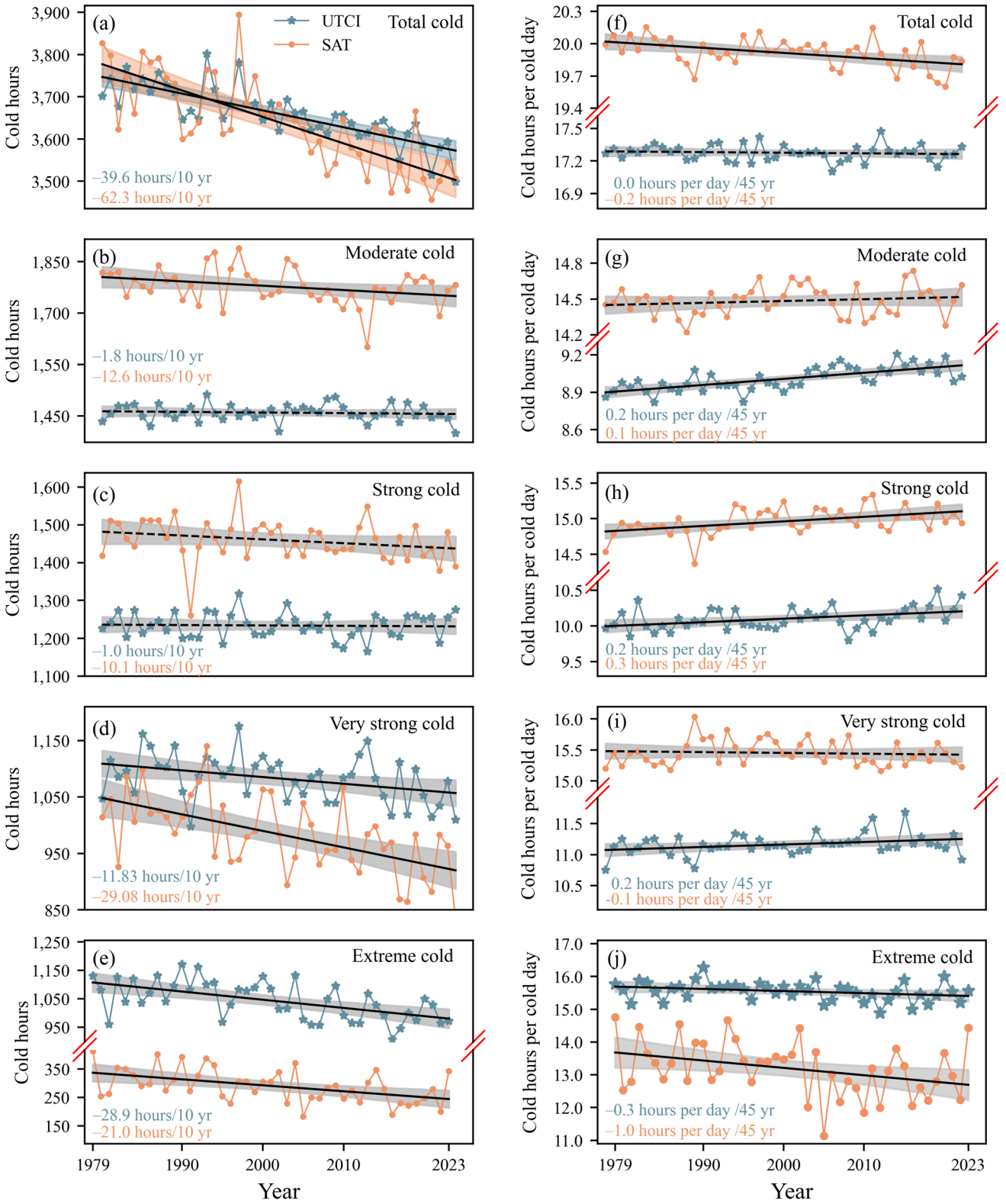

Fig. 1 Annual cold hours (left column) and cold hours per cold day (right column) across different cold stress categories, averaged over all global land (except the Antarctic) from 1979 to 2023. **a**, **f** Total cold stress (UTCI/SAT ≤ 0 °C). **b**, **g** Moderate cold stress (− 13 °C < UTCI/SAT ≤ 0 °C). **c**, **h** Strong cold stress (− 27 °C < UTCI/SAT ≤ − 13 °C). **d**, **i** Very strong cold stress (− 40 °C < UTCI/SAT ≤ − 27 °C). **e**, **j** Extreme cold stress (UTCI/SAT ≤ −40 °C). Solid/dashed black lines in **a**–**j** denote significant ($P < 0.05$)/insignificant ($P > 0.05$) trends derived using linear regression, and the shaded areas denote the corresponding 95% confidence interval. *UTCI* Universal Thermal Climate Index, *SAT* Surface air temperature.

were nonsignificant. Similarly, the SAT-based cold hours displayed a significant decrease for extreme and total cold, but an insignificant change or increase in the other three categories (Fig. 1f–j). The spatial distribution of cold hours within a single cold day exhibited notable shifts across various cold stress categories (Fig. S4[1]). In particular, for UTCI-based moderate cold stress, most regions exhibited significantly increased cold hours (Fig. S4c[1]). These results

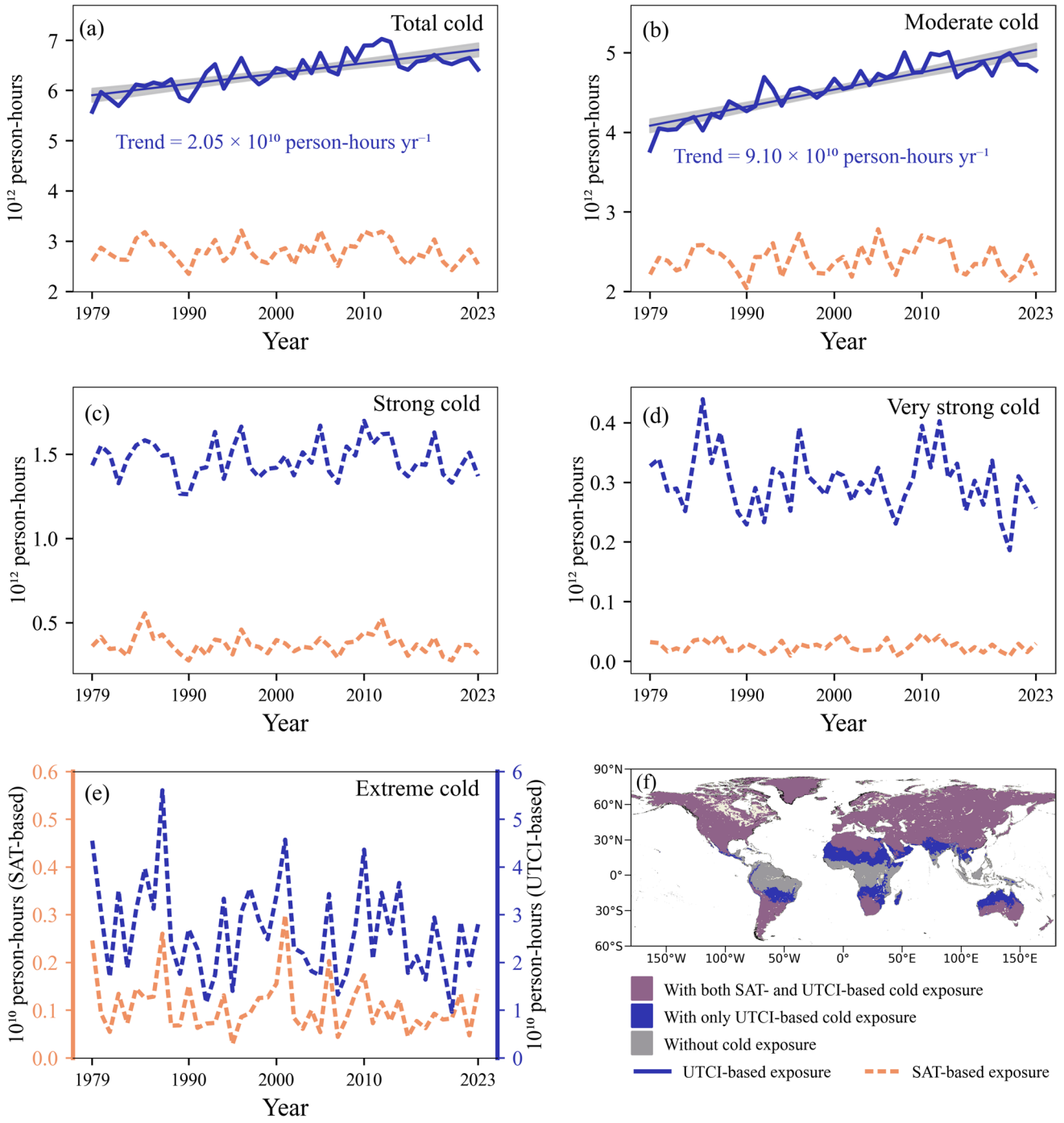

Fig. 2 Hourly population exposure to cold stress in different categories over global land during the period 1979–2023. **a** Total cold exposure. **b** Moderate cold exposure. **c** Strong cold exposure. **d** Very strong cold exposure. **e** Extreme cold exposure. **f** Spatial coverage of SAT- and UTCI-based cold exposure. The solid/dotted lines in **a**–**e** denote significant ($P < 0.05$)/insignificant ($P > 0.05$) trends derived using linear regression, and the shaded areas denote the corresponding 95% confidence interval. *UTCI* Universal Thermal Climate Index; *SAT* Surface air temperature.

indicate that changes in cold hours were not consistent with changes in cold days and did not decrease uniformly across different categories, but shifted from extreme/strong cold to strong/moderate cold with climate warming. This implies that daily cold stress indices may not capture the full extent of hourly-scale changes in cold stress.

The differences between UTCI- and SAT-based cold hours presented in Fig. 2 relate to the different meteorological variables considered in the two thermal metrics as well as the different spatial distributions of cold hours (Figs. S5 and S6[1]). The SAT-based cold only includes air temperature, while the UTCI also includes humidity, wind speed, and radiation. The grid mean of UTCI-based cold hours is also greater than that of SAT-based cold hours in all categories of cold stress (Figs. S5 and S6[1]).

3.2 Hourly Population Cold Exposure in Recent Decades

During the period 1979−2023, cold stress affected more than 60% of the global land area (81% for UTCI and 65% for SAT; Fig. 2f), and 40–70% of the global population experienced cold exposure (60–70% for UTCI and 40–50% for SAT). Although SAT-based hourly population cold exposure in all categories showed an insignificant change over recent decades, UTCI-based cold exposure in the categories of total and moderate cold stress exhibited a significant increase (Fig. 2a, b). The UTCI-based total cold exposure increased from 5.58×10^{12} person-hours in 1979 to 6.41×10^{12} person-hours in 2023, corresponding to an annual increment of 2.05×10^{10} person-hours yr^{-1} (Fig. 2a). Similar to the proportion of cold hours across categories (Fig. 1), moderate cold exposure accounted for roughly 70% of the total cold exposure (Fig. 2a, b).

The UTCI-based hourly population cold exposure is predominantly distributed across 30°−60°N, with high concentrations in North America, Europe, and central and eastern Asia (Fig. 3; Table S1[1]). The severity and spatial distribution of cold exposure varied with the category of cold stress, with significant changes in cold exposure observed in most cold-exposed areas (Fig. 3). The most significant increase in cold exposure was observed in northeast Asia, while the most significant decrease occurred in Europe (Fig. 3f–j). Due to the rate of increase outpacing the rate of decrease in cold exposure (Fig. 3f, g), global cold exposure in the categories of total and moderate cold has shown a significant increasing trend in recent decades (Fig. 2a, b). It is also evident that the increase in UTCI-based total cold exposure was mainly driven by moderate cold exposure (Fig. 3f, j). Similar spatial patterns were also found for SAT-based cold exposure (Fig. S7[1]).

At the national level, almost all inhabitants experienced cold stress in major cold-exposed countries (Table. S1[1]), with substantial discrepancies in population cold exposure among these countries (Tables S1 and S2[1]). In both UTCI- and SAT-based analyses, total cold exposures in China, Russia, and the United States accounted for over half of global cold exposure. The UTCI-/(SAT)-based annual means of total cold exposure in China, Russia, and the United States for the period 1979–2023 were 2.10×10^{12} (1.08×10^{12}), 6.55×10^{11} (4.49×10^{11}), and 6.04×10^{11} (2.62×10^{11}) person-hours, respectively. Additionally, the annual cold exposure per person (Sect. 2.6) also differed among countries, generally showing a latitude-dependent variation (Table S1[1]). This indicates the key role of regional climate and its associated changes in population cold exposure. In contrast to UTCI-derived cold exposure (Fig. 3), SAT-based cold exposure (Fig. S7[1]) features a lower intensity, and less pronounced temporal trends, demonstrating the critical influence of moisture, radiation, and wind speed in driving the rise in population cold exposure.

3.3 Cause of Increased Hourly Population Cold Exposure Under Climate Warming

By decomposing cold exposure as the climate, population, and interaction effects, we quantified their respective contributions to changes in cold exposure across various categories (see Sect. 2.7). Overall, the population effect outweighed the climate effect and served as the primary driver of UTCI-based global population cold exposure in all categories except for extreme cold during the period 1979−2023 (Fig. 4). However, the climate effect of changes in cold hours was also critical to changes in cold exposure in some areas, with large spatial discrepancies in the relative contributions of the two factors (climate and population) to changes in cold exposure. Population growth emerged as the primary driver of elevated UTCI-based total cold exposure in eastern and central Asia, and central parts of the United States during the period 1979−2023, whereas a reduction in cold hours accounted for the decline in cold exposure across Europe (Fig. 4).

Changes in both population (Fig. S8a[1]) and cold hours (Figs. S5 and S6[1]) in Europe were spatially heterogeneous. The decreased number of cold hours was the principal cause of decreased total exposure in western Europe, while both the decreased number of cold hours and negative population growth contributed to the decreased total cold exposure in eastern Europe (Figs. 3, 4). However, the interaction effect of population with climate exhibited little influence on changes in population cold exposures over the 1979−2023 period (Fig. 4). This is because the trends of the interaction effect and cold exposure exhibited opposing signs. For typical areas with increased cold exposure (for example, East Asia; Fig. 3f) and a decreased number of cold hours (for example, East Asia; Fig. S5b[1]), population growth was the

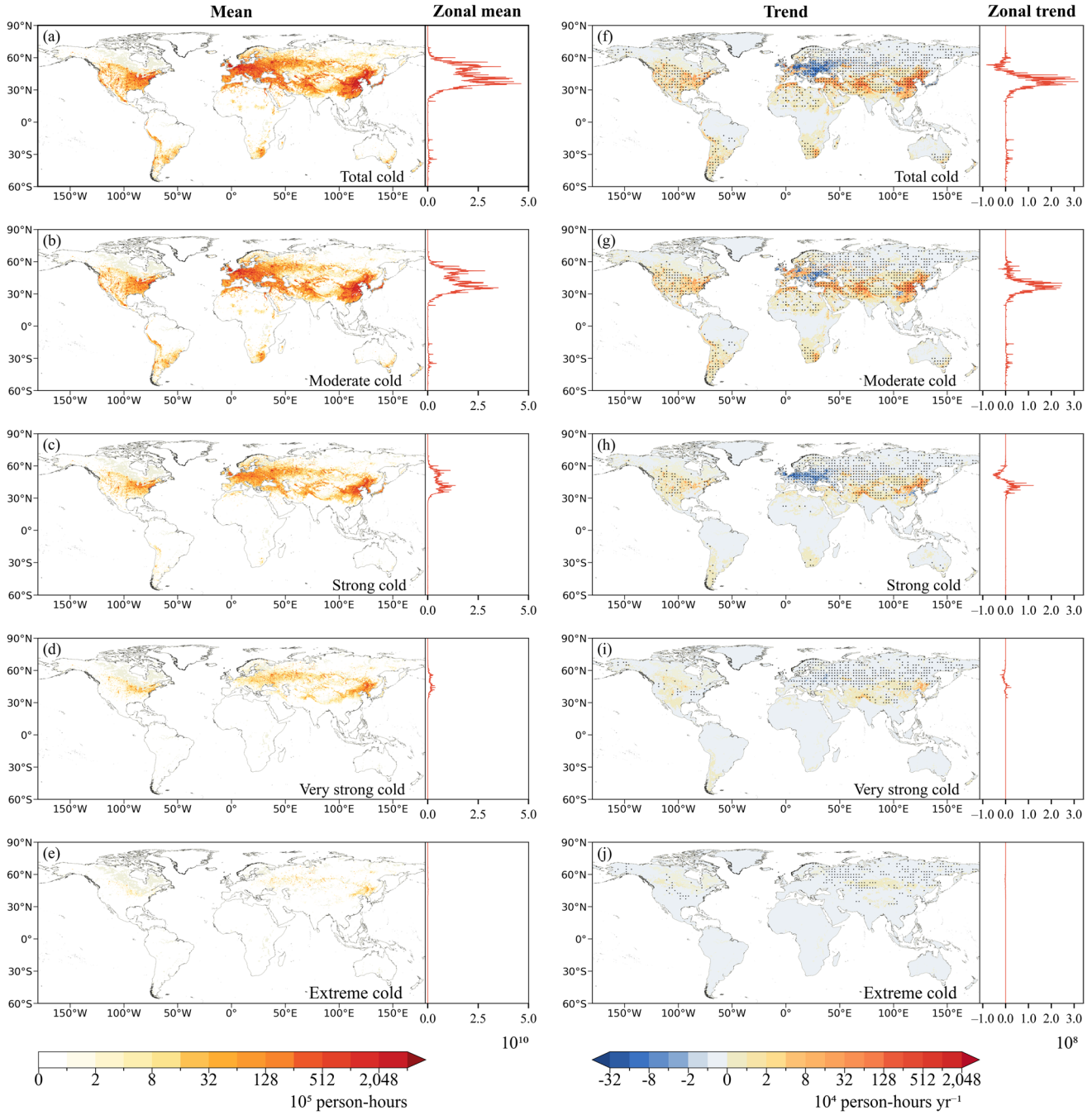

Fig. 3 **a**–**e** Spatial distributions of mean UTCI-based hourly population cold exposure and zonal averages for different cold stress categories from 1979 to 2023. **f**–**j** Spatial patterns of the trend and corresponding zonal sum trends for UTCI-based hourly population cold exposure in different categories from 1979 to 2023. **a**, **f** Total cold exposure. **b**, **g** Moderate cold exposure. **c**, **h** Strong cold exposure. **d**, **i** Very strong cold exposure. **e**, **j** Extreme cold exposure. Stippling in **f**–**j** denotes a significant trend ($P < 0.05$).

only contributing factor (that is, 100%) and the interaction effect, with a negative trend (see Sect. 2.7), had no contribution (that is, 0%) (Fig. 4b). For regions where cold exposure decreased (for example, Europe; Fig. 3f), the simultaneous decrease in both cold hours and population (Figs. S5b and S8a[1]) meant that the interaction effect, despite a positive trend, had no impact on the reduction of exposure (Fig. 4b).

The SAT-based attributions were similar to those based on UTCI, with the most evident discrepancy being the dominant factor contributing to moderate cold exposure in Europe (Fig. 4c, d). A decrease in the number of cold hours was the

main contributor to the decreased SAT-based moderate cold exposure, while negative population growth was the critical cause of the decreased UTCI-based moderate cold exposure. This divergence stems from the more rapid reduction compared to UTCI-based values (Figs. S5 and S6[1]), making the SAT-based climate effect more significant than the UTCI-based climate effect in Europe. This also implies that humidity, wind speed, and other meteorological variables exert a notable influence on cold exposure, especially in the more common moderate cold exposure category.

3.4 Implications of Hourly Population Cold Exposure and Its Current Risk

Given the potential link between population cold exposure and influenza (Carmona et al. 2016; Peci et al. 2019; Carter-Templeton et al. 2022), we investigated the relationship between the available weekly number of influenza cases from the FluNet dataset and weekly total cold exposure (see Sect. 2.8). Since China and the United States ranked highest in cold exposure (Table S1[1]) and had the most complete influenza case records in the FluNet dataset for the period 2015–2019, we chose these two countries to analyze the relationship between cold exposure and influenza. Increases in both SAT- and UTCI-based cold exposures were significantly correlated with the increased number of influenza cases in China and the United States.

This significant linear correlation was particularly evident during the cold seasons (that is, winter and spring) (Fig. 5a–d). Due to the unavailability of specific information regarding sentinel surveillance, we further investigated the relationship between influenza positivity rate and per capita cold hours to eliminate the influence of the number of sentinel sites on the sample size of influenza positives (Fig. S8b–S8e[1]). This provided the probability of an individual suffering from influenza when exposed to cold stress, and the same results were obtained as those shown in Fig. 5.

To explore future hourly population cold exposure and the associated risk, we projected global hourly population cold exposure until 2100 under the SSP2-4.5 scenario (Fig. 5e). To match the scenario of the population data, projected SAT data under the SSP2-4.5 scenario were used to cover the period 2015–2100 (O'Neill et al. 2016). Although the UTCI-based hourly cold exposure projection is limited due to the unavailability of data for the variables used in the calculation of the UTCI (see Sect. 2.1.2), the SAT-based projection showed that global hourly population cold exposure will not decline significantly in the near term (that is, until 2040). Regionally, hourly cold exposure is projected to continue increasing in the northern mid- and high-latitudes (Fig. S9[1]). The finding that moderate cold exposure represented 70% of the historical cold exposure and has increased significantly (Fig. 2) implies a probable widespread risk of moderate cold exposure for most populations in the near future. Moreover, given the greater UTCI-based total and moderate cold exposure compared to SAT-based total cold exposure in the historical period (Fig. 2a, b), the UTCI-based total and moderate cold exposure in the near future may also be greater than the SAT-based projection. This implies that the influenza risk related to hourly cold exposure will not decrease and may even increase, at least in the near future. These results emphasize that future climate warming will not lead to a decrease in current cold-related influenza and call for increased attention to this potential risk.

4 Discussion

Our research demonstrates that cold hours across various cold categories do not decrease uniformly; instead, there is a shift from extreme to moderate cold (Fig. 1). Notably, cold hours and cold days exhibit substantial discrepancies. Except for extreme cold hours, the number of cold hours per cold day has increased across all other categories (Fig. 1). Under global warming, cold exposure has increased significantly. This is mainly due to the rise in moderate cold exposure, while there is no significant decreasing trend in exposure at other categories. For hourly cold exposure in the future, although it will decrease significantly by 2100, there will not be a notable decline in the near future (that is, until around 2040). Furthermore, our results indicate that a robust linear association exists between influenza and hourly cold exposure, meaning that higher hourly cold exposure is associated with higher rates of influenza. This also indicates that the recent flu risk may not decrease with global warming.

Nevertheless, this study has several inherent limitations. First, the population data employed in our research are static and cannot characterize the dynamic changes in cold exposure driven by population movement and migration. Second, since the future hourly projections only have SAT, the projection of hourly UTCI-based cold hours cannot be calculated. Therefore, our estimation of future cold exposure is limited to the SAT. Furthermore, the spatiotemporal resolution of influenza data is at an annual national scale. Therefore, many factors related to influenza cannot be further analyzed. Moreover, the data records in many countries and regions are relatively incomplete. Therefore, we focused on China and the United States, two countries with large sample sizes and comprehensive data records, to analyze the potential relationship between cold exposure and influenza. This has certain limitations for the global estimation of this relationship. However, given that recent cold exposure may still increase, this qualitative relationship as an extended discussion and implication of cold exposure still holds certain reference significance.

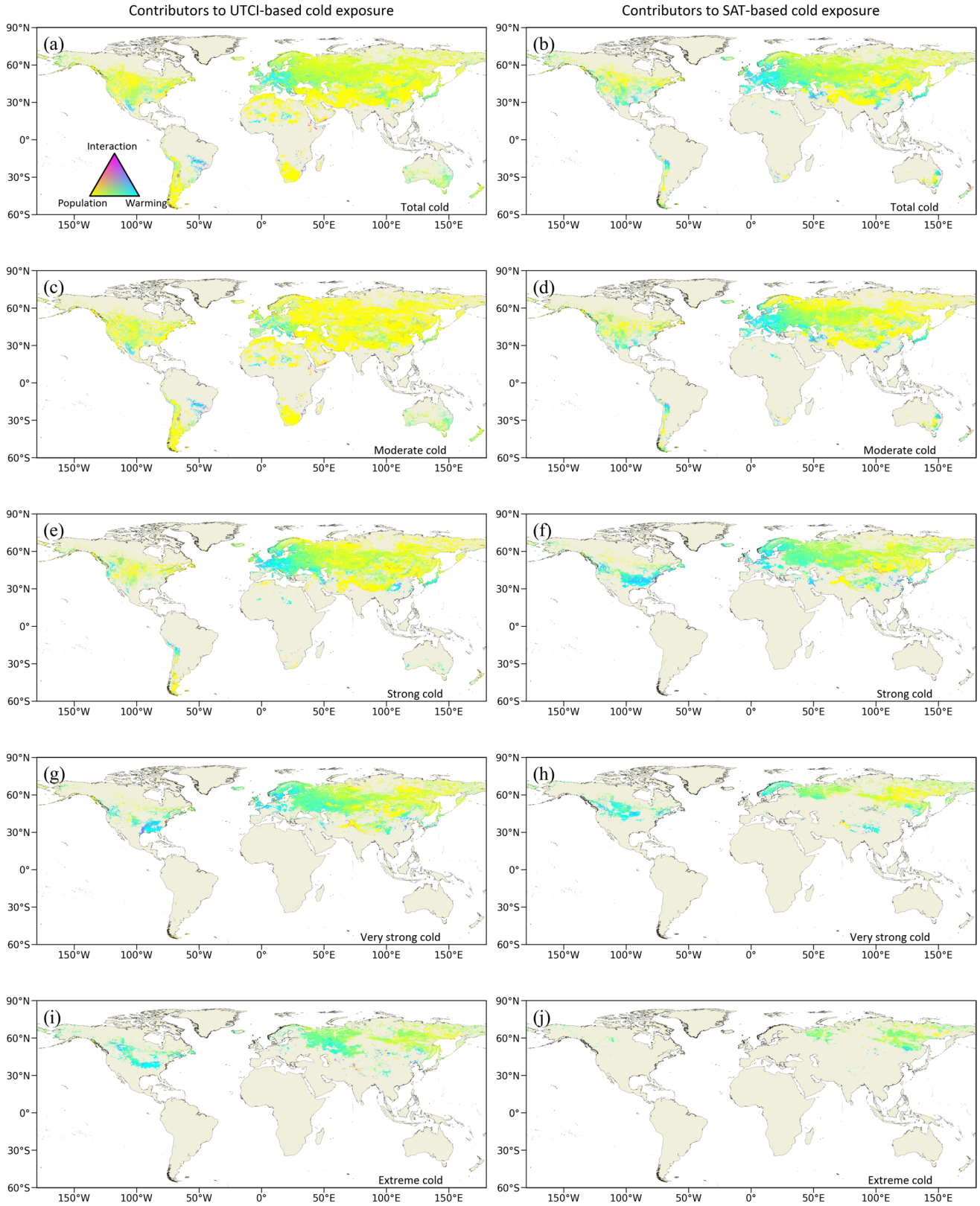

The relationship between influenza and cold exposure is relatively complex. In terms of temperature, the threshold sensitivity of influenza to temperature shows spatial heterogeneity. In South Korea, the risk of influenza significantly increases when the temperature is between 0 and 5 °C (Park et al. 2020), while in China, influenza peaks around

◂**Fig. 4** Contributions of climate, population, and interaction effects to the UTCI-based (left column) and SAT-based (right column) hourly population cold exposure in different cold stress categories from 1979 to 2023. **a**, **b** Total cold exposure. **c**, **d** Moderate cold exposure. **e**, **f** Strong cold exposure. **g**, **h** Very strong cold exposure. **i**, **j** Extreme cold exposure. The ratios of cyan, yellow, and magenta colors represent the quantitative contributions of the three effects, which are depicted within a color triangle. *UTCI* Universal Thermal Climate Index, *SAT* Surface air temperature.

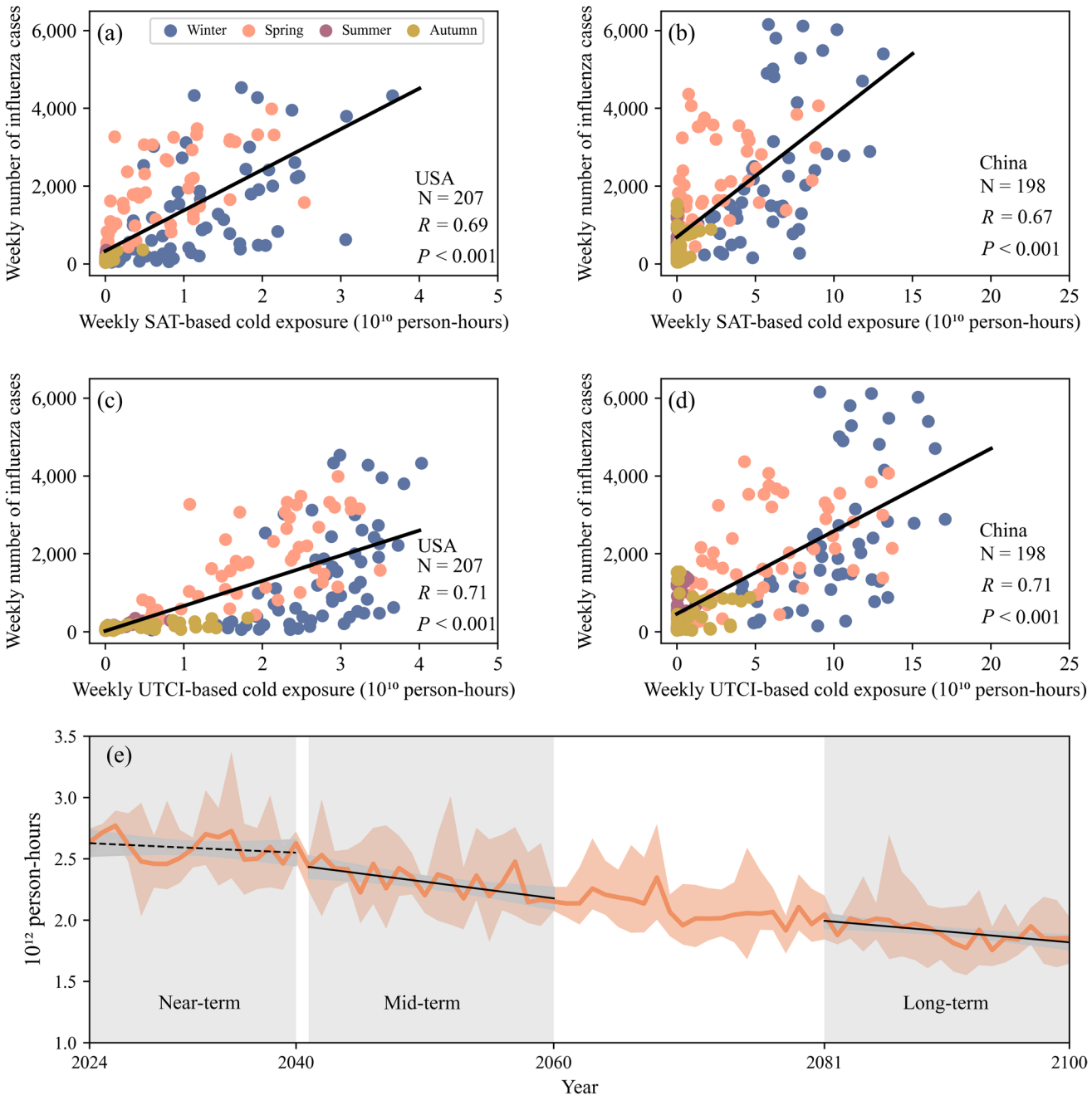

Fig. 5 Relationship between weekly number of influenza cases and weekly SAT-based **a**, **b** and UTCI-based **c**, **d** hourly cold exposure in the United States and China, alongside projected annual global population cold exposure derived from SAT-based hourly data from 2024 to 2100 **e**. Complete influenza datasets from 2015 to 2019 for the United States and China were utilized in **a**–**d** (see Sect. 2.3), with dot colors representing different seasons. *N*, *R*, and *P* in panels **a**–**d** denote the sample size, correlation coefficient, and significance level, respectively. The black lines in **a**–**d** are the linear regression fitting lines. The orange line and shaded area in **e** denote the annual cold exposure and its uncertainty based on simulated cold hours. Solid and dashed black lines in **e** denote statistically significant ($P < 0.05$) and non-significant ($P > 0.05$) trends from linear regression analyses, with the respective shaded areas indicating the 95% confidence intervals. *UTCI* Universal Thermal Climate Index; *SAT* Surface air temperature.

– 5 °C (Chen et al. 2021). The sensitivity of different viruses to temperature also varies. Previous studies have shown that influenza is not only related to cold exposure but also to humidity. Low temperature and relative humidity may provide a suitable environment for aerosol transmission, thereby enhancing the survival ability and transmission efficiency of influenza viruses (Lowen and Palese 2009). When the number of cold hours increases, people's outdoor activities tend to decrease, promoting individuals to spend more time indoors and thereby increasing the contact rate among people (Tamerius et al. 2011). Influenza is also influenced by economic development and population factors. The influenza rate among economically underdeveloped populations is significantly higher than that among populations of developed economies, and the infection rate among children is also relatively high (Balasegaram et al. 2012; Bota et al. 2021).

Considering the unevenness of cold exposure across different cold categories under climate warming and its significance for the prevention and treatment of influenza in the future, additional investigations into hourly cold exposure and its association with influenza are urgently required, necessitating the incorporation of multivariate regression (for example, with indoor behavior, vaccination rates, or socioeconomic factors) to isolate the specific effect of cold exposure. The cold exposure projection in this study is limited to SAT-based analysis, and UTCI-based cold exposure is highly expected. In this aspect, substantial progress in obtaining future meteorological forecast data related to perceived temperatures (such as UTCI) is needed. More precise data on influenza cases should also be accessible to further fill the research gap in this area.

Our research highlights that the changes in cold hours under climate warming is not uniform, and the cold hours varies disproportionately with the cold days. More importantly, cold exposure is still on the rise and is unlikely to decrease in the near future. This may pose challenges for future responses to cold exposure, such as heating, and the medical sector may bear considerable pressure. Thus, drawing on our findings, we recommend enhancing targeted attention to cold exposure risks in regions with substantial increases in such exposure.

5 Conclusion

This study uncovers changes of global hourly cold stress and cold exposure from 1979 to 2100. Cold stress did not decrease uniformly across all categories, with a notable shift from extreme to moderate cold exposure observed since 1979. The increase in cold exposure predominantly occurred in the middle and high latitudes of the Northern Hemisphere, particularly in regions like East Asia and North America, driven by population growth. A robust correlation was identified between hourly cold exposure, number of influenza cases, and influenza positivity rates. Projections of hourly cold exposure indicate that cold exposure will not start to decline until 2040, underscoring that cold exposure-related health hazards remain a critical concern requiring sustained attention. These findings show that current frameworks prioritizing extreme cold events may overlook risks from persistent moderate cold exposure, particularly in densely populated mid-latitude areas. Therefore, we suggest that assessments of cold exposure should consider the specific health impacts of cold stress in different categories and pay particular attention to regions experiencing a marked increase in exposure risk.

References

Arnold, C. 2022. Death by climate change. *Nature Climate Change* 12: 607–609.

Balasegaram, S., F. Ogilvie, A. Glasswell, C. Anderson, V. Cleary, D. Turbitt, and B. McCloskey. 2012. Patterns of early transmission of pandemic influenza in London – Link with deprivation. *Influenza and Other Respiratory Viruses* 6(3): e35–e41.

Ballester, J., X. Rodó, J. Robine, and F.R. Herrmann. 2016. European seasonal mortality and influenza incidence due to winter temperature variability. *Nature Climate Change* 6: 927–930.

Bota, A., M. Holmberg, L. Gardner, and M. Rosvall. 2021 Socioeconomic and environmental patterns behind H1N1 spreading in Sweden. *Scientific Reports* 11: Article 22512.

Brimicombe, C., C. Di Napoli, T. Quintino, F. Pappenberger, R. Cornforth, and H.L. Cloke. 2022 Thermofeel: A Python thermal comfort indices library. *SoftwareX* 18: Article 101005.

Broadbent, A.M., E.S. Krayenhoff, and M. Georgescu. 2020. The motley drivers of heat and cold exposure in 21st century US cities. *Proceedings of the National Academy of Sciences* 117: 21108–21117.

Bröde, P., D. Fiala, K. Błażejczyk, I. Holmér, G. Jendritzky, B. Kampmann, B. Tinz, and G. Havenith. 2012. Deriving the operational procedure for the Universal Thermal Climate Index (UTCI). *International Journal of Biometeorology* 56: 481–494.

Cannon, A.J., S.R. Sobie, and T.Q. Murdock. 2015. Bias correction of GCM precipitation by quantile mapping: How well do methods preserve changes in quantiles and extremes?. *Journal of Climate* 28: 6938–6959.

Carmona, R., J. Díaz, I.J. Mirón, C. Ortiz, M.Y. Luna, and C. Linares. 2016. Mortality attributable to extreme temperatures in Spain:

A comparative analysis by city. *Environment International* 91: 22–28.

Carter-Templeton, H., G.F. Templeton, L.H. Nicoll, L. Maxie, T.S. Kittle, S.A. Jasko, E.E. Carpenter, and K.A. Monsen. 2022. Associations between weather-related data and influenza reports: A pilot study and related policy implications. *Applied Nursing Research* 67: Article 151413.

Chen, C., D.X. Jiang, D.Y. Yan, L.C. Pi, X.B. Zhang, Y.X. Du, X.X. Liu, and M. Yang et al. 2023. The global region-specific epidemiologic characteristics of influenza: World Health Organization FluNet data from 1996 to 2021. *International Journal of Infectious Diseases* 129: 118–124.

Chen, C., X. Zhang, D. Jiang, D. Yan, Z. Guan, Y. Zhou, X. Liu, C. Huang, et al. 2021. Associations between temperature and influenza activity: A national time series study in China. *International Journal of Environmental Research and Public Health* 18: Article 10846.

Christiansen, B., C. Alvarez-Castro, N. Christidis, A. Ciavarella, I. Colfescu, T. Cowan, J. Eden, and M. Hauser et al. 2018. Was the cold European winter of 2009/10 modified by anthropogenic climate change? An attribution study. *Journal of Climate* 31: 3387–3410.

CMA (China Meteorological Administration). 2017. *Specifications for surface meteorological observation*. Beijing: China Meteorological Press (in Chinese).

Collins, K.J., J.C. Easton, H. Belfield-Smith, A.N. Exton-Smith, and R.A. Pluck. 1985. Effects of age on body temperature and blood pressure in cold environments. *Clinical Science* 69: 465–470.

Cosgrove, B.A., D. Lohmann, K.E. Mitchell, P.R. Houser, E.F. Wood, J.C. Schaake, A. Robock, C.H. Marshall, et al. 2003. Real-time and retrospective forcing in the North American Land Data Assimilation System (NLDAS) project. *Journal of Geophysical Research: Atmospheres* 108: Article 2002JD003118.

Di Napoli, C., C. Barnard, C. Prudhomme, H.L. Cloke, and F. Pappenberger. 2020. Thermal comfort indices derived from ERA5 reanalysis. Copernicus Climate Change Service (C3S), Climate Data Store (CDS).

Donaldson, G.C., V.E. Tchernjavskii, S.P. Ermakov, K. Bucher, and W.R. Keatinge. 1998. Winter mortality and cold stress in Yekaterinburg, Russia: Interview survey. *BMJ* 316: 514–518.

Du, Y.J., M. Jing, C.M. Lu, J.R. Zong, L.L. Wang, and Q. Wang. 2022. Global population exposure to extreme temperatures and disease burden. *International Journal of Environmental Research and Public Health* 19: Article 13288.

Dunne, J.P., L.W. Horowitz, A.J. Adcroft, P. Ginoux, I.M. Held, J.G. John, J.P. Krasting, S. Malyshev, et al. 2020. The GFDL Earth System Model Version 4.1 (GFDL-ESM 4.1): Overall coupled model description and simulation characteristics. *Journal of Advances in Modeling Earth Systems* 12: Article e2019MS002015.

Ebi, K.L., A. Capon, P. Berry, C. Broderick, R.D. Dear, G. Havenith, Y. Honda, and R.S. Kovats et al. 2021. Hot weather and heat extremes: Health risks. *The Lancet* 398: 698–708.

Eyring, V., S. Bony, G.A. Meehl, C.A. Senior, B. Stevens, R.J. Stouffer, and K.E. Taylor. 2016. Overview of the Coupled Model Intercomparison Project Phase 6 (CMIP6) experimental design and organization. *Geoscientific Model Development* 9: 1937–1958.

Ference, R.S., A.L. James, and H.D. Stupak. 2020. Physiologic model for seasonal patterns in flu transmission. *The Laryngoscope* 130: 309–313.

Fiala, D., G. Havenith, P. Bröde, B. Kampmann, and G. Jendritzky. 2012. UTCI-Fiala multi-node model of human heat transfer and temperature regulation. *International Journal of Biometeorology* 56: 429–441.

Frieler, K., S. Lange, F. Piontek, C.P.O. Reyer, J. Schewe, L. Warszawski, F. Zhao, and L. Chini et al. 2017. Assessing the impacts of 1.5 °C global warming – Simulation protocol of the Inter-Sectoral Impact Model Intercomparison Project (ISIMIP2b). *Geoscientific Model Development* 10: 4321–4345.

Fyke, J., and A. Weaver. 2023. Reducing personal climate risk to reduce personal climate anxiety. *Nature Climate Change* 13: 209–210.

Gao, X.J., J. Wu, Y. Shi, J. Wu, Z.Y. Han, D.F. Zhang, Y. Tong, and R.K. Li et al. 2018. Future changes in thermal comfort conditions over China based on multi-RegCM4 simulations. *Atmospheric and Oceanic Science Letters* 11: 291–299.

Gasparrini, A., Y.M. Guo, M. Hashizume, E. Lavigne, A. Zanobetti, J. Schwartz, A. Tobias, and S. Tong et al. 2015. Mortality risk attributable to high and low ambient temperature: A multicountry observational study. *The Lancet* 386: 369–375.

Geiger, T., J. Gütschow, D.N. Bresch, K. Emanuel, and K. Frieler. 2021. Double benefit of limiting global warming for tropical cyclone exposure. *Nature Climate Change* 11: 861–866.

Gelaro, R., W. McCarty, M.J. Suárez, R. Todling, A. Molod, L. Takacs, C.A. Randles, and A. Darmenov et al. 2017. The Modern-Era Retrospective Analysis for Research and Applications, Version 2 (MERRA-2). *Journal of Climate* 30: 5419–5454.

Hajima, T., M. Watanabe, A. Yamamoto, H. Tatebe, M.A. Noguchi, M. Abe, R. Ohgaito, and A. Ito et al. 2020. Development of the MIROC-ES2L Earth system model and the evaluation of biogeochemical processes and feedbacks. *Geoscientific Model Development* 13: 2197–2244.

Havenith, G., D. Fiala, K. Błazejczyk, M. Richards, P. Bröde, I. Holmér, H. Rintamaki, and Y. Benshabat et al. 2012. The UTCI-clothing model. *International Journal of Biometeorology* 56: 461–470.

Hersbach, H., B. Bell, P. Berrisford, S. Hirahara, A. Horányi, J.M. Sabater, J. Nicolas, C. Peubey, et al. 2020. The ERA5 global reanalysis. *Quarterly Journal of the Royal Meteorological Society* 146. Wiley: 1999–2049.

Jones, N. 2021. Why easing COVID restrictions could prompt a fierce flu rebound. *Nature* 598(7881): 395.

Jones, B., B.C. O'Neill, L. McDaniel, S. McGinnis, L.O. Mearns, and C. Tebaldi. 2015. Future population exposure to US heat extremes. *Nature Climate Change* 5: 652–655.

Kovats, R.S., and S. Hajat. 2008. Heat stress and public health: A critical review. *Annual Review of Public Health* 29: 41–55.

Li, M.Y., W. Fang, R.L. Meng, J.X. Hu, G.H. He, Z.L. Hou, M.G. Zhou, C. Zhou, et al. 2023. The comparison of mortality burden between exposure to dry-cold events and wet-cold events: A nationwide study in China. *Science of the Total Environment* 904: Article 166859.

Lowen, A., and P. Palese. 2009. Transmission of influenza virus in temperate zones is predominantly by aerosol, in the tropics by contact: A hypothesis. *PLoS Currents* 1. https://doi.org/10.1371/currents.rrn1002.

Luo, B.K., P.J. Minnett, M. Szczodrak, N.R. Nalli, and V.R. Morris. 2020. Accuracy assessment of MERRA-2 and ERA-Interim sea surface temperature, air temperature, and humidity profiles over the Atlantic Ocean using AEROSE measurements. *Journal of Climate* 33: 6889–6909.

Martínez-Solanas, È., M. Quijal-Zamorano, H. Achebak, D. Petrova, J. Robine, F.R. Herrmann, X. Rodó, and J. Ballester. 2021. Projections of temperature-attributable mortality in Europe: A time series analysis of 147 contiguous regions in 16 countries. *The Lancet Planetary Health* 5: e446–e454.

Mora, C., B. Dousset, I.R. Caldwell, F.E. Powell, R.C. Geronimo, C.R. Bielecki, C.W.W. Counsell, and B.S. Dietrich et al. 2017. Global risk of deadly heat. *Nature Climate Change* 7: 501–506.

O'Neill, B.C., C. Tebaldi, D.P.V. Vuuren, V. Eyring, P. Friedlingstein, G. Hurtt, R. Knutti, and E. Kriegler et al. 2016. The Scenario Model Intercomparison Project (ScenarioMIP) for CMIP6. *Geoscientific Model Development* 9: 3461–3482.

Oudin Åström, D., B. Forsberg, K.L. Ebi, and J. Rocklöv. 2013. Attributing mortality from extreme temperatures to climate change in Stockholm, Sweden. *Nature Climate Change* 3: 1050–1054.

Park, J.E., W.-S. Son, Y. Ryu, S.B. Choi, O. Kwon, and I. Ahn. 2020. Effects of temperature, humidity, and diurnal temperature range on influenza incidence in a temperate region. *Influenza and Other Respiratory Viruses* 14: 11–18.

Paschalidou, A.K., P.A. Kassomenos, and G.R. McGregor. 2017. Analysis of the synoptic winter mortality climatology in five regions of England: Searching for evidence of weather signals. *Science of the Total Environment* 598: 432–444.

Patz, J.A., D. Campbell-Lendrum, T. Holloway, and J.A. Foley. 2005. Impact of regional climate change on human health. *Nature* 438: 310–317.

Peci, A., A.L. Winter, Y. Li, S. Gnaneshan, J. Liu, S. Mubareka, and J.B. Gubbay. 2019. Effects of absolute humidity, relative humidity, temperature, and wind speed on influenza activity in Toronto, Ontario, Canada. *Applied and Environmental Microbiology* 85: Article e02426-18.

Pennisi, E. 2020. Living with heat. *Science* 370: 778–781.

Peterson, T.C., R.R. Heim, R. Hirsch, D.P. Kaiser, H. Brooks, N.S. Diffenbaugh, R.M. Dole, and J.P. Giovannettone et al. 2013. Monitoring and understanding changes in heat waves, cold waves, floods, and droughts in the United States: State of knowledge. *Bulletin of the American Meteorological Society* 94: 821–834.

Raatikka, V.P., M. Rytkönen, S. Näyhä, and J. Hassi. 2007. Prevalence of cold-related complaints, symptoms and injuries in the general population: The FINRISK 2002 cold substudy. *International Journal of Biometeorology* 51: 441–448.

Romanello, M., C.D. Napoli, C. Green, H. Kennard, P. Lampard, D. Scamman, M. Walawender, and Z. Ali et al. 2023. The 2023 report of the Lancet Countdown on health and climate change: The imperative for a health-centred response in a world facing irreversible harms. *The Lancet* 402: 2346–2394.

Roussel, M., D. Pontier, J.M. Cohen, B. Lina, and D. Fouchet. 2016. Quantifying the role of weather on seasonal influenza. *BMC Public Health* 16: Article 441.

Shaman, J., and M. Kohn. 2009. Absolute humidity modulates influenza survival, transmission, and seasonality. *Proceedings of the National Academy of Sciences* 106: 3243–3248.

Sheridan, S.C., and M.J. Allen. 2015. Changes in the frequency and intensity of extreme temperature events and human health concerns. *Current Climate Change Reports* 1: 155–162.

Shi, J., L.L. Cui, Y. Ma, H.Q. Du, and K.M. Wen. 2018. Trends in temperature extremes and their association with circulation patterns in China during 1961–2015. *Atmospheric Research* 212: 259–272.

Tamerius, J., M.I. Nelson, S.Z. Zhou, C. Viboud, M.A. Miller, and W.J. Alonso. 2011. Global influenza seasonality: Reconciling patterns across temperate and tropical regions. *Environmental Health Perspectives* 119: 439–445.

The Eurowinter Group. 1997. Cold exposure and winter mortality from ischaemic heart disease, cerebrovascular disease, respiratory disease, and all causes in warm and cold regions of Europe. *Lancet* 349: 1341–1346.

Tuholske, C., K. Caylor, C. Funk, A. Verdin, S. Sweeney, K. Grace, P. Peterson, and T. Evans. 2021. Global urban population exposure to extreme heat. *Proceedings of the National Academy of Sciences* 118: Article e2024792118.

van Oldenborgh, G.J., E. Mitchell-Larson, G.A. Vecchi, H. de Vries, R. Vautard, and F. Otto. 2019. Cold waves are getting milder in the northern midlatitudes. *Environmental Research Letters* 14: Article 114004.

Wen, A., T.H. Wu, X.D. Wu, X.F. Zhu, R. Li, J. Ni, G.J. Hu, Y.P. Qiao, et al. 2022. Evaluation of MERRA-2 land surface temperature dataset and its application in permafrost mapping over China. *Atmospheric Research* 279: Article 106373.

Woodhouse, P.R., K.T. Khaw, and M. Plummer. 1993. Seasonal variation of blood pressure and its relationship to ambient temperature in an elderly population. *Journal of hypertension* 11: 1267–1274.

World Health Organization. 2022. *Global Influenza Programme*. Washington, DC: World Health Organization.

Zhang, Y., Q.Z. Li, Y. Ge, X. Du, and H.Y. Wang. 2022. Growing prevalence of heat over cold extremes with overall milder extremes and multiple successive events. *Communications Earth & Environment* 3: Article 73.

Zhang, P.F., G.Y. Ren, Y. Xu, X.L.L. Wang, Y. Qin, X.B. Sun, and Y.Y. Ren. 2019. Observed changes in extreme temperature over the global land based on a newly developed station daily dataset. *Journal of Climate* 32: 8489–8509.

Zhang, Y.W., X.F. Wang, Y.F. Li, and J.Q. Ma. 2019. Spatiotemporal analysis of influenza in China, 2005–2018. *Scientific Reports* 9: Article 19650.

Zhao, Q., Y.M. Guo, T.T. Ye, A. Gasparrini, S.L. Tong, A. Overcenco, A. Urban, and A. Schneider et al. 2021. Global, regional, and national burden of mortality associated with non-optimal ambient temperatures from 2000 to 2019: A three-stage modelling study. *The Lancet Planetary Health* 5: e415–e425.

Zhu, H., and J. Duan. 2025. Inverted age-pyramidal global hourly population heat exposure. *Environmental Research Letters* 20: Article 124072.